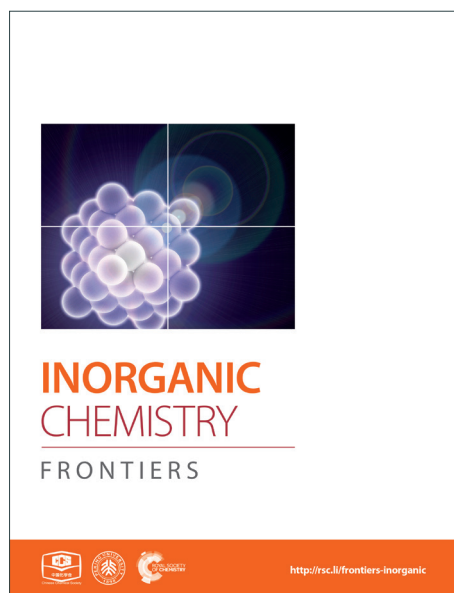
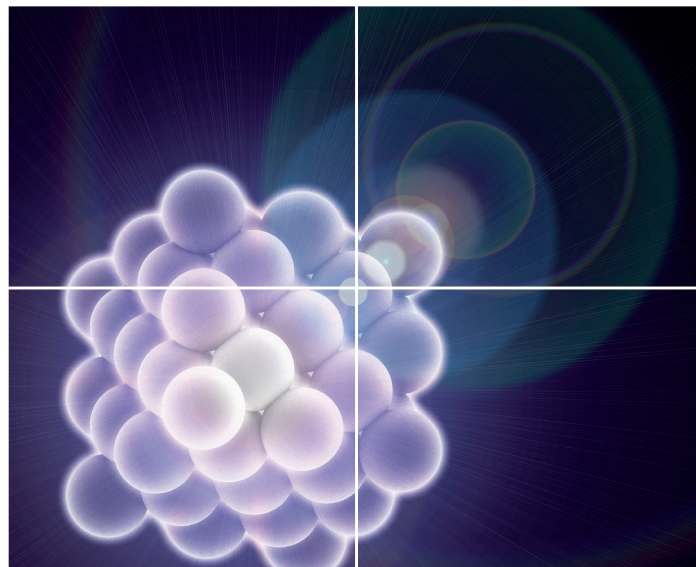


INORGANIC CHEMISTRY

FRONTIERS

Accepted Manuscript



This is an *Accepted Manuscript*, which has been through the Royal Society of Chemistry peer review process and has been accepted for publication.

Accepted Manuscripts are published online shortly after acceptance, before technical editing, formatting and proof reading. Using this free service, authors can make their results available to the community, in citable form, before we publish the edited article. We will replace this *Accepted Manuscript* with the edited and formatted *Advance Article* as soon as it is available.

You can find more information about *Accepted Manuscripts* in the [Information for Authors](#).

Please note that technical editing may introduce minor changes to the text and/or graphics, which may alter content. The journal's standard [Terms & Conditions](#) and the [Ethical guidelines](#) still apply. In no event shall the Royal Society of Chemistry be held responsible for any errors or omissions in this *Accepted Manuscript* or any consequences arising from the use of any information it contains.

COMMUNICATION

Cite this: DOI: 10.1039/x0xx00000x

Hierarchical Nanoarray Materials for Advanced Nickel-Zinc Batteries

Received 00th January 2012,

Accepted 00th January 2012

Zhiyi Lu^{†a}, Xiaochao Wu^{†a}, Xiaodong Lei^a, Yaping Li^a and Xiaoming Sun^{*a}

DOI: 10.1039/x0xx00000x

www.rsc.org/

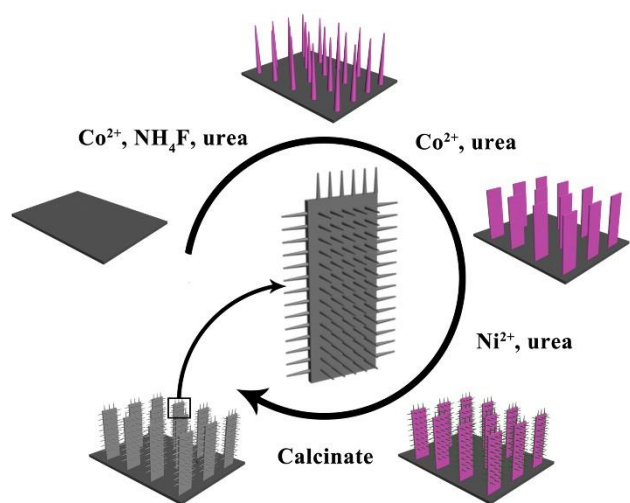
In this work we report a hierarchical Co₃O₄@NiO nanostrips@nanorods arrays (Co₃O₄@NiO NSRAs) which is directly grown on three-dimensional conductive substrates by a facile three-step hydrothermal reaction and a following annealing treatment. This hierarchical structure provides several advantages including a large contact surface area, short ion diffusion path and good charge transport, which validate this film as an advanced electrode for nickel-zinc battery with both high energy density (5.1 mWh cm⁻²) and power density (82.2 mW cm⁻²).

The need for the development of efficient energy storage devices with high safety for electrical vehicles as well as portable electronics is becoming more and more urgent.^{1,4} Lithium ion batteries (LIBs) have attracted the widest attention due to the high energy density, however, the flammability of organic electrolytes and high reactivity of Li containing electrode materials will inevitably induce unsafe factors, which limit the widespread usage of LIBs.^{5, 6} Aqueous rechargeable batteries (such as Ni-Zn battery,^{7, 8} Ni-MH battery,^{9, 10} and Ni-Fe battery^{11, 12}), which usually show much higher power density and safety, have attracted renewed interest as a possible alternative solution. Aqueous Ni-Zn battery, where both Zn²⁺/Zn and Ni²⁺/Ni³⁺ conversion processes occur associated with water molecular, is thought of an advance energy storage system due to its relatively higher theoretical specific energy density (~372 Wh kg⁻¹), high open-circuit voltage, low toxicity and cost.^{7, 13}

For the NiZn battery system, the anode material is metallic Zn while the cathode material usually shows a much weaker conductivity (typically Ni(OH)₂), which would significantly affect the electron transportation through the electrode with a high mass-loading, thus degrading the overall energy storage performance, including the specific capacity and rate capability. In order to improve the performance, the structure and morphology of the active materials should be further explored and optimized.¹⁴⁻¹⁶

Herein we designed and fabricated hierarchical Co₃O₄@NiO nanostrips@nanorods arrays (Co₃O₄@NiO NSRAs) as positive electrodes for Ni-Zn batteries. The NiO nanorods were uniformly and vertically grown outside of the Co₃O₄ nanostrip arrays, leading to the formation of a hierarchical structure. As demonstrated previously,¹⁶⁻²¹ constructing hierarchical nanoarray structure was considered as an effective approach to achieve high utilization of the electrode material, because it not only facilitated the electron transport and electrolyte penetration, but also showed a synergistic effect of each component, thereby bringing about a boost improvement of capacitive performance. This hierarchical architecture showed a high areal capacity (~2.91 mAh cm⁻²), excellent rate capability (retains ~61% of the capacity at 10 times higher current density), and prominent cycling stability (~96% after 1000 cycles), which were benefited from the high mass-loading and high porosity of the active materials, and the direct contact to the current collector underlying. Besides, we paired the Co₃O₄@NiO NSRAs with a zinc anode in alkaline solution as a NiZn battery system, which delivered a peak energy density of ~5.12 mWh cm⁻² and a peak power density of ~82.21 mW cm⁻², respectively. The charge and discharge cycling stability of the battery showed a capacity degradation of ~10% over 500 cycles at 50 mA cm⁻² and The columbic efficiency of the battery was found greater than 97%, which were both receivable for an aqueous rechargeable battery system.

The fabrication process of the Co₃O₄@NiO NSRAs was illustrated in Scheme 1. The nickel foam was chosen here as the substrate because of its zig-zag skeleton and high porosity, which helped to increase the active surface area.²² Co₂(OH)₂CO₃ nanowires were firstly grown on the nickel foam to form a well-aligned array-like structure.^{23, 24} Afterwards, the Co₂(OH)₂CO₃ nanowires were converted into Co(OH)₂ nanostrips by a secondary hydrothermal treatment, which dissolved and recrystallized the precursor nanowires.²⁵ Thirdly, the Ni²⁺ salt was subsequently added and precipitated to obtain a hierarchical structure. It is notable that the film was bonded tightly to the foam substrate, as even hours of ultrasonication did not dislodge the colored material from the foam. Finally, the precursor hierarchical nanostrips@nanorods arrays were annealed to convert into the corresponding oxides materials.



Scheme 1. Schematic illustration of the fabrication procedures of hierarchical $\text{Co}_3\text{O}_4@/\text{NiO}$ NSRAs.

The surface morphology of the hierarchical structure was firstly investigated by scanning emission microscopy (SEM). The surface morphologies of the samples after the 1st and 2nd growth step were shown in Figure S1, revealing nanowire arrays (NWAs) and nanostrip arrays (NSAs) were successfully fabricated on the substrate. After Ni(II) salt precipitation and thermal treatment, hierarchical structures with multidirectional nanorods could be seen on the nanostrips, thus forming a highly dense film (Figures 1A and B). The resulting NSRAs were vertically aligned on the substrate and the total size of the assembled structure was in the range of 2–4 μm while its thickness was about 400 nm. The average diameter and length of the nanorods were estimated to be about 10–15 nm and 100–200 nm, respectively.

High resolution TEM image (Figure 1C) was further measured to gain more structural information. Two lattice spacings (0.237 nm and 0.277 nm), corresponding to the (111) plane of NiO and (220) plane of NiCo_2O_4 were observed in an individual nanorod, indicating that the tip was composed of NiO and the root was mainly made of spinel-type mixed metal oxides.¹⁷ Only the spinel phase was found in the XRD pattern (Figure 1D), suggesting that the NiO nanorods were poorly crystallized with small crystal grains, which was consistent with the HRTEM results. X-ray photoelectron spectroscopy (XPS, Figure S2) demonstrated the +2 oxidation state of Ni and mixed oxidation state (2+ and 3+) of Co with a Ni/Co ratio of 4, while the energy dispersive spectroscopy (EDS, Figure S3) result showed a much smaller Ni/Co ratio of 2.5:1, thus confirming the vast majority of the materials in the surface of the hierarchical structure (i.e. the tip of the secondary nanorod) was NiO.

The electrochemical properties of the $\text{Co}_3\text{O}_4@/\text{NiO}$ NSRAs were examined by cyclic voltammetry (CV) and charge/discharge measurements using a standard three electrode system in 6 M KOH. The representative CV curves at scan rates of 1, 5 and 10 mV s^{-1} were shown in Figure 2A, where a pair of obvious redox peaks was observed. It was attributed to the redox couples of $\text{Ni}^{2+}/\text{Ni}^{3+}$ and $\text{Co}^{2+}/\text{Co}^{3+}$,^{17, 26} which located at similar equilibrium potentials ($\Delta E < 0.1$ V), thus leading to the formation of overlapped and broad peaks. As the sweep rate was increased, the anodic peak potential and cathodic peak potential shifted to more anodic and cathodic directions, respectively, and this phenomenon might be caused by the polarization effect including concentration

polarization and resistance effect. The typical charge and discharge profiles of the NSRAs at different current densities were presented in Figure 2B. It can be observed that the voltage plateaus were located between 0.2 V and 0.3 V in the discharge curves, in consistent with the position of the anodic peak in CV curves. The symmetric shape of charge and discharge process illustrated the high coulombic efficiency of the electrode material (at least 95% for various current densities). Calculated from the discharge curves (Figure 2C), the areal capacity delivered as high as 2.91 mAh cm^{-2} (corresponding to a specific capacity of ~ 242.4 mAh g^{-1}) at a current density of 5 mA cm^{-2} , while the capacity could be retained at 1.76 mAh cm^{-2} as the current density increased to 50 mA cm^{-2} , showing a rate capability of $\sim 60.5\%$. The remarkable rate capability as well as the ultrahigh areal capacity manifested the effectiveness of constructing ordered hierarchical mesoporous architecture. For comparison purposes, the Co_3O_4 NWAs and NSAs after 1st and 2nd growth step and annealing process were evaluated using similar measurements (Figure S4). It was found that both Co_3O_4 NWAs and NSAs showed much inferior performance, which indicated that the addition of NiO and the hierarchical construction were both beneficial for achieving high areal and specific capacity.

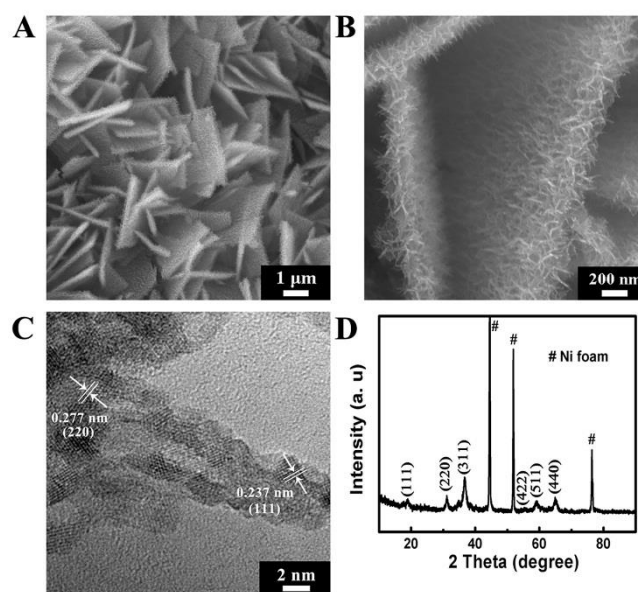


Figure 1. (A) and (B), SEM images of the hierarchical $\text{Co}_3\text{O}_4@/\text{NiO}$ NSRAs with different magnifications; (C) and (D), HRTEM image and XRD pattern of the hierarchical $\text{Co}_3\text{O}_4@/\text{NiO}$ NSRAs.

Long-term cycling stability is another essential factor for practical application. Over 1000 cycles charge/discharge testing was employed to examine the service life of the $\text{Co}_3\text{O}_4@/\text{NiO}$ NSRAs electrode at a current density of 50 mA cm^{-2} (Figure 2D). The specific capacity decreased slightly ($\sim 4\%$) over the initial 100 cycles and subsequently remained essentially unchanged over the following 900 cycles. Moreover, the coulombic efficiency of the electrode gradually increased and maintained at $\sim 98\%$ upon cycling testing. The high stability indicated that the charge/ discharge processes did not induce structural change of the electrodes which would influence the surface redox reactions. Combination of the above features (high areal capacity, remarkable rate capability and excellent stability) was attributed to the hierarchical structure design with the integration of unique merits of Co_3O_4 nanostrips as scaffold to render fast electron transport and superior electrolyte diffusion and ultrathin NiO

nanorods with high electrochemically active surface area, thus leading to substantially improved capacitive and rate performance.

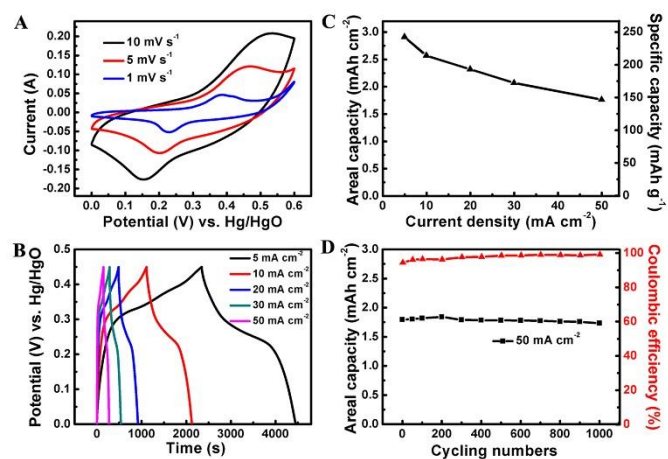
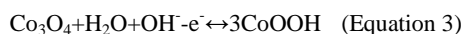
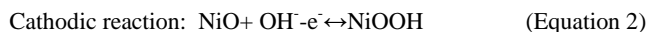
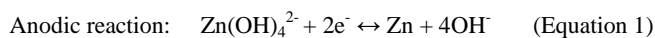


Figure 2. (A) and (B) The CV curves and the galvanostatic charge and discharge curves of the hierarchical $\text{Co}_3\text{O}_4@\text{NiO}$ NSRAs; (C) areal and specific capacitances the hierarchical $\text{Co}_3\text{O}_4@\text{NiO}$ NSRAs at different current densities; (D) cycling stability and coulombic efficiency of the hierarchical $\text{Co}_3\text{O}_4@\text{NiO}$ NSRAs at 50 mA cm^{-2} .

The potential application of the $\text{Co}_3\text{O}_4@\text{NiO}$ NSRAs in aqueous NiZn batteries was further investigated by incorporation of zinc as the anode (Figure 3A). An aqueous solution of 6 M KOH saturated with ZnO was used as the electrolyte. Copper foil was used as both the current collector and substrate for electrodeposition of Zn. The CV curves of the NiZn battery at various scan rates were shown in Figure 3B, where a pair of redox peaks was observed. These peaks corresponded to the following reactions.^{8, 27}



To quantitatively measure the energy storage performance of the NiZn battery, galvanostatic charge/discharge curves at different current densities was performed (Figure 3C). The calculated specific capacity of the aqueous NiZn battery was $\sim 2.89 \text{ mAh cm}^{-2}$ (or 182.6 mAh g^{-1}) at a current density of 5 mA cm^{-2} , and it was still maintained at as high as $\sim 1.28 \text{ mAh cm}^{-2}$ (or 80.5 mAh g^{-1}) when the current density was increased to 50 mA cm^{-2} . Together with the high operating voltage ($\sim 1.7 \text{ V}$), this NiZn battery showed comparable or higher energy density and power density comparing with other batteries reported^{7, 28-30}, as shown in the Ragone plot in Figure 3D. This NiZn battery could deliver an areal energy density of 5.12 mWh cm^{-2} at a power density of 8.61 mW cm^{-2} , and an energy density of 2.11 mWh cm^{-2} at a power density of 82.21 mW cm^{-2} . Although the high areal energy density was partially by virtue of the high mass-loading, the calculated specific energy density and power density ($215.51 \text{ Wh kg}^{-1}$ and 3.45 kW kg^{-1}) were still comparable or higher to the previous data.^{7, 13, 31} To demonstrate the practical application of the battery, we engineered a pouch cell of our samples, which was used to light a commercial light-emitting diode (LED) (Fig. S5). The tandem aqueous batteries (two devices connected in series) could easily light up a LED for hours after being fully charged.

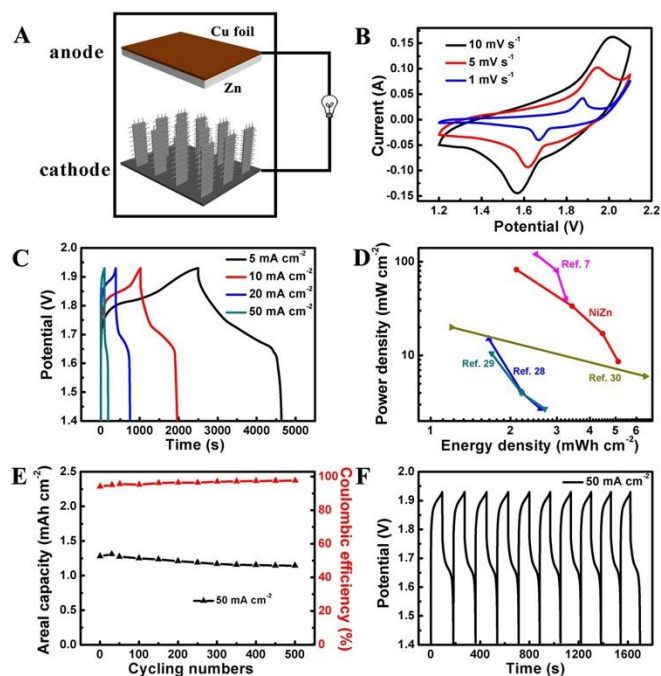


Figure 3. (A) Schematic representation of the novel NiZn battery; (B) and (C) the CV curves and galvanostatic charge and discharge curves of the NiZn battery; (D) the Ragone plots of the NiZn battery in comparison with other batteries reported; (E) and (F), cycling stability, coulombic efficiency and the last several cycling curves of the NiZn battery at 50 mA cm^{-2} .

The long-term stability was also examined by cycling testing, as shown in Figure 3E and F. Unlike to the highly stable $\text{Co}_3\text{O}_4@\text{NiO}$ NSRAs electrodes, the NiZn battery showed a quasi-stable performance with a capacity degradation of $\sim 11\%$ after 500 cycles. This was attributed to the Zn dendrite formation on the Cu substrate^{32, 33}, which might result in decreasing the effective working area and decelerating the Zn deposition process. The SEM images of the Zn electrode after first 5 cycles and 500 cycling test are shown in Fig. S6. Notably, the coulombic efficiency of the battery could achieve above 97% during the cycling testing at high rate, illustrating the good reversibility.

In summary, we have developed a multi-step hydrothermal reaction and a following calcination process to fabricate hierarchical $\text{Co}_3\text{O}_4@\text{NiO}$ NSRAs directly grown on conductive substrate. Due to the unique architecture, the hierarchical nanoarrays exhibited an outstanding capacitive performance as the positive electrodes. Moreover, by incorporating a zinc anode, an aqueous NiZn battery was fabricated, which delivered both high energy density and power density. This study not only provides a battery technology with the advantages of high energy and power density, cost-effectiveness and high safety, but also clearly demonstrates the feasibility of constructing hierarchical nanoarrays on a variety of energy storage applications.

This work was supported by the National Natural Science Foundation of China, the 973 Program (2011CBA00503 and 2011CB932403), the Program for New Century Excellent Talents in

Universities, and the Program for Changjiang Scholars and Innovative Research Team in University.

Notes and references

^a State Key Laboratory of Chemical Resource Engineering, Beijing University of Chemical Technology, Beijing 100029, China
Tel.: +86-10-64448751. Fax: +86-10-64425385.

E-mail: sunxm@mail.buct.edu.cn

† Contributed equally to this work

Electronic Supplementary Information (ESI) available: [experimental section, XPS survey, SEM, EDS and XRD results, electrochemical testing results]. See DOI: 10.1039/c000000x/

1. C. Liu, F. Li, L. P. Ma and H. M. Cheng, *Adv. Mater.*, 2010, **22**, E28-62.
2. J. Jiang, Y. Li, J. Liu, X. Huang, C. Yuan and X. W. Lou, *Adv. Mater.*, 2012, **24**, 5166-5180.
3. A. L. Mohana Reddy, S. R. Gowda, M. M. Shaijumon and P. M. Ajayan, *Adv. Mater.*, 2012, **24**, 5045-5064.
4. H. Wang and H. Dai, *Chem. Soc. Rev.*, 2013, **42**, 3088-3113.
5. P. Poizot, S. Laruelle, S. Grugeon, L. Dupont and J.-M. Tarascon, *Nature* 2000, **407**, 496-499.
6. X. Zhou, L. J. Wan and Y. G. Guo, *Adv. Mater.*, 2013, **25**, 2152-2157.
7. M. Gong, Y. Li, H. Zhang, B. Zhang, W. Zhou, J. Feng, H. Wang, Y. Liang, Z. Fan, J. Liu and H. Dai, *Energy Environ. Sci.*, 2014, **7**, 2025-2032.
8. X. Fan, Z. Yang, R. Wen, B. Yang and W. Long, *J. Power Sources*, 2013, **224**, 80-85.
9. B. Li, H. Cao, J. Shao, H. Zheng, Y. Lu, J. Yin and M. Qu, *Chem Commun (Camb)*, 2011, **47**, 3159-3161.
10. Y. Liu, H. Pan, M. Gao and Q. Wang, *J. Mater. Chem.*, 2011, **21**, 4743.
11. H. Wang, Y. Liang, M. Gong, Y. Li, W. Chang, T. Mefford, J. Zhou, J. Wang, T. Regier, F. Wei and H. Dai, *Nat. Commun.*, 2012, **3**, 917.
12. C. Long, T. Wei, J. Yan, L. Jiang and Z. Fan, *ACS Nano*, 2013, **7**, 11325-11332.
13. M. Ma, J. P. Tu, Y. F. Yuan, X. L. Wang, K. F. Li, F. Mao and Z. Y. Zeng, *J. Power Sources*, 2008, **179**, 395-400.
14. R. K. Joshi and J. J. Schneider, *Chem. Soc. Rev.*, 2012, **41**, 5285-5312.
15. Z.-S. Wu, G. Zhou, L.-C. Yin, W. Ren, F. Li and H.-M. Cheng, *Nano Energy*, 2012, **1**, 107-131.
16. C. K. Chan, H. Peng, G. Liu, K. McIlwrath, X. F. Zhang, R. A. Huggins and Y. Cui, *Nature Nanotech.*, 2008, **3**, 31-35.
17. Z. Lu, Q. Yang, W. Zhu, Z. Chang, J. Liu, X. Sun, D. G. Evans and X. Duan, *Nano Res.*, 2012, **5**, 369-378.
18. Q. Yang, Z. Lu, T. Li, X. Sun and J. Liu, *Nano Energy*, 2014, **7**, 170-178.
19. H. Chen, L. Hu, M. Chen, Y. Yan and L. Wu, *Adv. Funct. Mater.*, 2014, **24**, 934-942.
20. L. Hu, W. Chen, X. Xie, N. Liu, Y. Yang, HuiWu, Y. Yao, M. Pasta, H. N. Alshareef and Y. Cui, *ACS Nano*, 2011, **5**, 8904-8913.
21. W. Chen, R. B. Rakhi, L. Hu, X. Xie, Y. Cui and H. N. Alshareef, *Nano Lett.*, 2011, **11**, 5165-5172.
22. J. Wang, H. X. Zhong, Y. L. Qin and X. B. Zhang, *Angew. Chem. Int. Ed. Engl.*, 2013, **52**, 5248-5253.
23. Q. Yang, Z. Lu, Z. Chang, W. Zhu, J. Sun, J. Liu, X. Sun and X. Duan, *RSC Adv.*, 2012, **2**, 1663.
24. W. Zhu, Z. Lu, G. Zhang, X. Lei, Z. Chang, J. Liu and X. Sun, *J. Mater. Chem. A*, 2013, **1**, 8327.
25. Q. Yang, Z. Lu, X. Sun and J. Liu, *Sci. Rep.*, 2013, **3**, 3537.
26. F. Zhang, C. Yuan, J. Zhu, J. Wang, X. Zhang and X. Lou, *Adv. Funct. Mater.*, 2013, **23**, 3909-3915.
27. B. Yang, Z. Yang and R. Wang, *J. Power Sources*, 2014, **251**, 14-19.
28. K. Sun, T. S. Wei, B. Y. Ahn, J. Y. Seo, S. J. Dillon and J. A. Lewis, *Adv. Mater.*, 2013, **25**, 4539-4543.
29. K. Yoshima, H. Munakata and K. Kanamura, *J. Power Sources*, 2012, **208**, 404-408.
30. A. M. Gaikwad, G. L. Whiting, D. A. Steingart and A. C. Arias, *Adv. Mater.*, 2011, **23**, 3251-3255.
31. J. Jindra, *J. Power Sources*, 2000, **88**, 202-205.
32. Y. Li and H. Dai, *Chem. Soc. Rev.*, 2014, **43**, 5257-5275.
33. Y. Li, M. Gong, Y. Liang, J. Feng, J. E. Kim, H. Wang, G. Hong, B. Zhang and H. Dai, *Nat. Commun.*, 2013, **4**, 1805.